Materials International
Open-Access Journal (ISSN: 2668-5728)

Article
Volume 8, Issue 1, 2026, 10
https://doi.org/10.33263/Materials81.010

ZnO Nanoparticles Modified by *Citrus aurantium* Oil Show Anti-Tumor Effects in a Murine Model of Ehrlich Ascites Carcinoma

Amr S. Eissa [1,*], Lamiaa A. A. Barakat [1], Nasser Mohammed Hosny [1], Amira A. Awadalla [2]

[1] Chemistry Department, Faculty of Science, Port Said University, POB 42522 Port Said, Egypt; amr.salem@sci.psu.edu.eg (A.S.E.); l.abdelatef@sci.psu.edu.eg (L.A.A.B.); nasser_hosny@sci.psu.edu.eg (N.M.H.);
[2] Center of Excellence for Genome and Cancer Research, Urology and Nephrology Center, Mansoura University, Mansoura 35516, Egypt; a.awadallah@mans.edu.eg (A.A.A.);
* Correspondence: amr.salem@sci.psu.edu.eg;

Received: 9.04.2025; Accepted: 4.02.2026; Published: 10.03.2026

Abstract: This study investigates the therapeutic efficacy of zinc oxide nanoparticles (ZnO NPs) and *Citrus aurantium* oil–functionalized ZnO NPs (CAO-ZnO NPs) in a murine model of Ehrlich ascites carcinoma (EAC). Following tumor induction, mice were administered intraperitoneal treatments of ZnO NPs or CAO-ZnO NPs over a three-week period. Both nanoparticle formulations elicited a significant reduction in tumor volume; however, the CAO-ZnO NP–treated group exhibited a more pronounced antitumor response. Moreover, treated animals demonstrated improved hepatic and renal function, accompanied by enhanced antioxidant defense mechanisms, as evidenced by elevated glutathione (GSH) and superoxide dismutase (SOD) levels, alongside reduced markers of oxidative stress, including lipid peroxidation and nitric oxide. Collectively, these results indicate that CAO-ZnO NPs represent a promising nanotherapeutic approach capable of inhibiting tumor progression while preserving vital organ function.

Keywords: ZnO nanoparticles; cancer, anti-tumor; *Citrus aurantium* CAO; mice.

1. Introduction

Cancer progresses when normal regulatory mechanisms of the cell are disrupted, leading to uncontrolled proliferation of abnormal cells that may invade nearby tissues and disseminate to distant organs via the blood and lymphatic circulations. This pathological process can occur in nearly any tissue, disrupting the tightly regulated balance of cell division that maintains normal growth and repair [1]. Worldwide, cancer continues to be one of the leading causes of death and represents a major public health challenge.

According to data from the World Health Organization (WHO, 2019), cancer represents the first or second leading cause of death before the age of 70 in over 60% of countries. In many regions, its mortality rate surpasses that of other major diseases, including cardiovascular disorders [2].

Conventional chemotherapy, including alkylating agents, antimetabolites, and targeted biological therapies, does not always achieve complete remission. Because of their limited selectivity, these therapeutic agents often cause systemic toxicities, including

immunosuppression, neurotoxicity, and cardiotoxicity, which limit their broader clinical use [3]. Consequently, there is an urgent need to develop more targeted and biocompatible anticancer modalities.

Zinc oxide nanoparticles (ZnO NPs) have been recognized as promising nanotherapeutic systems due to their superior cytotoxicity against malignant cells. Their anticancer activity is mainly attributed to the generation of reactive oxygen species (ROS), which encourage oxidative stress, inflammatory alterations, and mitochondrial dysfunction, ultimately leading to apoptosis or necrosis [4]. However, ZnO NPs may also exert cytotoxic effects on normal tissues in a dose-dependent manner, largely due to uncontrolled Zn^{2+} ion release and excessive ROS accumulation [5]. This dualistic behavior underscores the necessity for structural or surface modifications to enhance their selectivity and biosafety.

Recently, surface modification of ZnO NPs with plant-derived bioactive constituents has involved increasing interest as an approach to improve therapeutic performance while reducing toxicity. *Citrus aurantium* (bitter orange) is a phytochemically rich plant that contains flavonoids, alkaloids, and coumarins with documented antioxidant, antimicrobial, and antiproliferative activities. Although plant-mediated synthesis of nanoparticles has been widely examined, the application of Citrus aurantium essential oil (CAO) in the green production and optimization of ZnO NPs for cancer therapy remains poorly explored.

In the present study, we synthesized CAO-functionalized ZnO nanoparticles (CAO-ZnO NPs). We evaluated their antitumor potential, hepatic and renal safety profiles, and modulatory effects on oxidative stress in a murine model of Ehrlich ascites carcinoma (EAC). By integrating the bioactive constituents of CAO with the intrinsic anticancer properties of ZnO NPs, this work aims to overcome the limitations of conventional nanotherapeutic systems. These findings support the potential of a biocompatible plant-based nanoplatform with improved tumor cell activity and lower systemic toxicity, offering a promising strategy in cancer nanomedicine [6].

2. Materials and Methods

2.1. Chemicals.

2.1.1. Extraction of *C. aurantium* aqueous peel extracts.

Citrus aurantium CAO (CAO), natural, cold-compressed, California origin, FG was kindly supplied by Merck (Sigma-Aldrich). Used for the synthesis of ZnONPs [6].

2.2. Green synthesis of zinc oxide nanoparticles.

A solution was prepared by dissolving 2.2 g of zinc acetate dihydrate [$Zn(OAc)_2 \cdot 2H_2O$] in 100 mL of distilled water and 0.4 g of sodium hydroxide (NaOH) in 30 mL of distilled water. The NaOH solution was then added dropwise to the zinc acetate solution under continuous vigorous stirring at 60°C for 12 hours [7]. Upon completion, the reaction mixture was cooled to room temperature, and the resulting precipitate was collected by centrifugation at 10,000 rpm for 30 minutes. The obtained zinc oxide precipitate was thoroughly washed with distilled water and dried at 60°C.

To incorporate *Citrus aurantium* essential oil (CAO) and facilitate ZnO nanoparticle synthesis, 1 mL of CAO was introduced into the reaction mixture described above. After

drying, a yellow powder was obtained, indicating the successful formation of CAO-functionalized ZnO nanoparticles.

This synthesis procedure was previously employed to produce ZnO nanoparticles modified with CAO, and the results confirmed the effective loading of CAO onto the ZnO surface [8]. Characterization of the synthesized nanoparticles was conducted using Fourier-transform infrared spectroscopy (FT-IR), ultraviolet–visible spectroscopy (UV–Vis), X-ray diffraction (XRD), transmission electron microscopy (TEM), selected area electron diffraction (SAED), and high-resolution transmission electron microscopy (HRTEM) to validate nanostructure formation and confirm CAO incorporation [8].

According to the referenced study [8], XRD, TEM, HRTEM, and SAED analyses confirmed the formation of hexagonal ZnO nanoparticles with an average crystallite size of approximately 13 nm. Upon CAO loading, the nanoparticles exhibited a rod-like morphology with an average particle size of about 34 nm. The optical band gap values were determined to be 3.4 eV for pure ZnO NPs and 3.7 eV for CAO-functionalized ZnO NPs, respectively [8].

2.3. Experimental animals.

Thirty mature female albino mice, aged 7–10 weeks and weighing between 25 and 35 g, were housed at a density of four animals per polycarbonate cage. The mice were maintained under standardized laboratory conditions, including a 12-hour light/dark cycle, controlled temperature (24°C), and relative humidity of 50–70%. Standard laboratory chow and water were provided *ad libitum* throughout the experimental period. All animal care and experimental procedures were conducted in accordance with the guidelines of the National Institutes of Health (NIH) for the care and use of laboratory animals and were approved by the Institutional Animal Ethics Committee of the Faculty of Science, Port Said University.

2.4. Cancer induction.

An Ehrlich ascites carcinoma (EAC) cell line was utilized in the present study. The original cell line was obtained from the National Cancer Institute, Cairo University, Egypt. EAC cells were collected *via* intraperitoneal (i.p.) aspiration using a sterile insulin syringe, and the sample was subsequently diluted with 0.9% sterile saline at a ratio of 1:9 (v/v). Cell viability and density (cells/mL) were determined using a hemocytometer under a light microscope following staining with trypan blue dye to distinguish viable from non-viable cells [9]. For tumor induction, approximately 1×10^6 viable EAC cells suspended in 0.1 mL of phosphate-buffered saline (PBS) were intraperitoneally injected into each mouse to establish a liquid tumor model [10].

2.5. Animal groups.

Mice were subcutaneously inoculated in the right hind limb (thigh) with 0.1 mL of a suspension containing 5×10^5 viable Ehrlich ascites carcinoma (EAC) cells per mouse. The day of tumor inoculation was designated as day 0. After one week, the animals were randomized and divided into three experimental groups (n = 10 per group) as follows:

Control (EAC-bearing) group: Mice in this group received intraperitoneal (i.p.) injections of 1×10^6 EAC cells suspended in 0.1 mL of phosphate-buffered saline (PBS) once daily for three consecutive weeks [11].

ZnO NP-treated group: Mice received zinc oxide nanoparticles (ZnO NPs) suspended in deionized water at a dose of 50 mg/kg body weight *via* i.p. injection once daily for three consecutive weeks following EAC implantation [11].

CAO–ZnO NP-treated group: Mice were administered *Citrus aurantium* oil–functionalized zinc oxide nanoparticles (CAO–ZnO NPs) at a dose of 50 mg/kg body weight *via* i.p. injection once daily for three consecutive weeks following EAC implantation [11].

2.6. Mean survival time.

Mean survival time was calculated according to the following formulas [12]. Mean survival time (MST) = ∑ Survival time (days) of each mouse in a group/ Total number of mice.

2.7. Collection of blood and tissue samples.

At the conclusion of the experimental period, all mice were weighed, and blood samples were collected *via* cardiac puncture under inhalational general anesthesia. The obtained blood was centrifuged to separate the serum, which was subsequently stored at −20°C for biochemical analyses. Following sample collection, the animals were humanely euthanized by cervical dislocation. Tumor masses were then excised, weighed, and fixed in buffered formalin for subsequent histopathological examination.

2.8. Detection of liver and kidney enzymes.

Alanine Transaminase (ALT), Aspartate Aminotransferase (AST), blood urea, and serum creatinine were measured in serum using an RT ELISA kit (Cusabio, USA) by using an Infinite F50 microplate Reader (Tecan, Mannedorf, Switzerland).

2.9. Evaluation of oxidative stress status.

Tumor tissues were analyzed to determine catalase (CAT) activity, malondialdehyde (MDA) concentration, reduced glutathione (GSH) level, superoxide dismutase (SOD) activity, and nitric oxide (NO) content. Tissue samples were weighed, finely minced, and homogenized, followed by centrifugation at 10,000 × g for 15 minutes. The resulting supernatants were used for biochemical assays. All parameters were quantified according to the manufacturer's protocols using commercial colorimetric assay kits (Bio-Diagnostics, Giza, Egypt).

2.10. ELISA assays.

The effects of CAO-functionalized zinc oxide nanoparticles (CAO–ZnO NPs) on apoptotic and inflammatory mediators were evaluated by quantifying specific biomarkers using enzyme-linked immunosorbent assay (ELISA). Apoptotic markers included B-cell lymphoma 2 (BCL-2) (Rat BCL-2 ELISA Kit; MyBioSource, Inc., USA; catalog no. MBS704330), caspase-3 (Rat Caspase-3 ELISA Kit; MyBioSource, Inc., USA; catalog no. MBS700575), and annexin A5 (Rat ANXA5 ELISA Kit; Novus Biologicals, USA; catalog no. NBP2-68230). The inflammatory marker tumor necrosis factor-alpha (TNF-α) was quantified using a Rat TNF-α ELISA Kit (Elabscience, China; catalog no. E-EL-R2856). All assays were performed according to the manufacturer's protocols.

2.11. Histological studies.

Ehrlich ascites carcinoma (EAC) tumor tissues were fixed in buffered formalin and subsequently embedded in paraffin. Paraffin-embedded tissue blocks were sectioned at a thickness of 5 µm and stained with hematoxylin and eosin (H&E). The stained sections were then dehydrated, mounted with coverslips, and examined under a light microscope (Olympus, Japan) for histopathological evaluation.

2.12. Statistical analysis.

Statistical analyses were performed using SPSS software, version 26 (IBM Corp., Chicago, IL, USA). Quantitative data were expressed as mean ± standard deviation (SD) and compared among the three experimental groups using one-way analysis of variance (ANOVA), followed by Tukey's post hoc test for multiple comparisons. A two-tailed *p*-value of less than 0.05 was considered statistically significant.

2.13. Physicochemical characterization of ZnONPs and CAO-ZnONPs.

The synthesized ZnO nanoparticles (ZnO NPs) and *Citrus aurantium* oil–functionalized ZnO nanoparticles (CAO–ZnO NPs) were characterized using Fourier-transform infrared spectroscopy (FT-IR), ultraviolet–visible (UV–Vis) spectroscopy, X-ray diffraction (XRD), transmission electron microscopy (TEM), high-resolution transmission electron microscopy (HRTEM), and selected area electron diffraction (SAED), as summarized in Table 1.

Table 1. summarizes key physicochemical parameters.

Property	ZnONPs	CAO-ZnONPs
Average particle size (TEM)	13 nm	34 nm (rod-shaped)
Zeta potential	−18.2 mV	−25.7 mV
Crystallinity (XRD phase)	Hexagonal wurtzite	Hexagonal wurtzite
Optical band gap (UV–Vis)	3.4 eV	3.7 eV
Surface functional groups (FTIR)	Zn–O stretch, OH peaks	CAO peaks + Zn–O

3. Results and Discussion

This study describes the synthesis and characterization of ZnO nanoparticles functionalized with Citrus aurantium oil. Since both ZnO and Citrus aurantium oil possess anticancer properties, loading ZnO nanoparticles with CAO was expected to enhance their antitumor activity. To investigate this hypothesis, the cytotoxic and antioxidant effects of CAO-loaded ZnO nanoparticles were evaluated using HePG-2 and HCT-116 cell lines. Figure 1 illustrates the overall experimental design and biological evaluation workflow.

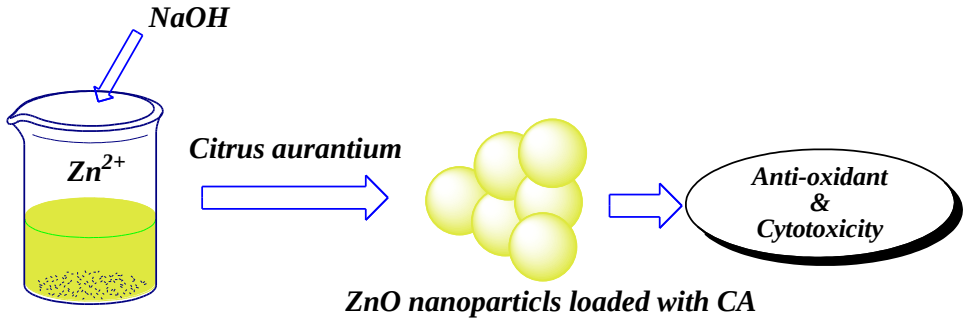

Figure 1. Graphical representation of the synthetic and biological methodology used for ZnO and its effect on cancer cells in mice.

3.1. Determination of oxidative stress markers.

As shown in Table 2, treatment with both ZnO NPs and CAO–ZnO NPs resulted in a significant reduction in malondialdehyde (MDA) levels, indicating decreased oxidative stress. Concurrently, elevated levels of reduced glutathione (GSH) and superoxide dismutase (SOD) were observed, reflecting enhanced antioxidant activity in the treated groups. Moreover, nitric oxide (NO) and catalase (CAT) activities exhibited significant increases following nanoparticle administration, with the most pronounced effects observed in the CAO–ZnO NP–treated group. Figure 2 shows oxidative stress markers in the different studied groups

Table 2. Oxidative stress markers in the different studied groups.

Parameter	Control group	ZnONPs-	CAO. ZnONPs	P value	Post hoc analysis
MDA (nmol/g. tissue)	11.2±1.4	6.1±0.92	3.6±0.61	**P<0.001**	**P1<0.001** P2=0.003 **P3<0.001**
GSH (mmol/g. tissue)	0.96±0.07	1.6±0.18	1.7±0.05	**P<0.001**	**P1<0.001** P2=0.093 **P3<0.001**
SOD (U/g. tissue)	29.6±4.9	64.8±5.1	82.3±5	**P<0.001**	**P1<0.001** **P2<0.001** **P3<0.001**
NO (µmol/g. tissue)	2.7±0.4	1.7±0.12	1.4±0.13	**P<0.001**	**P1<0.001** P2=0.156 **P3<.001**
CAT (U/g. tissue)	0.25±0.19	0.82±0.1	0.94±0.04	**P<0.001**	**P1<0.001** P2=0.296 **P3<0.001**

MDA: Malondialdehyde;
GSH: Reduced glutathione;
SOD: Superoxide dismutase;
NO: Nitric oxide;
CAT: Catalase.
ZnONPs: Zinc oxide nanoparticles.
CAO-ZnONPs: Citrus aurantium oil-loaded zinc oxide nanoparticles.
P1: Comparison between the control group and the ZnONPs group.
P2: Comparison between the ZnONPs group and the CAO-ZnONPs group.
P3: Comparison between the CAO-ZnONPs group and the control group

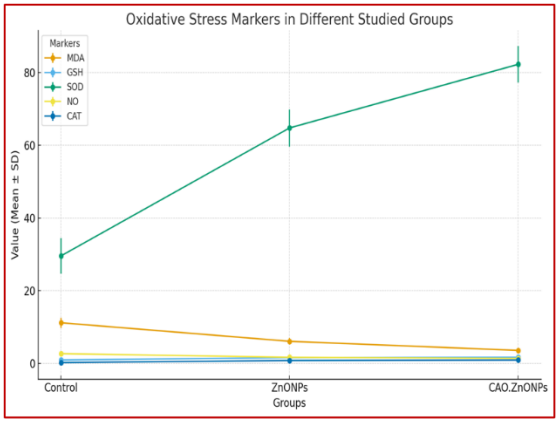

Figure 2. A chart showing oxidative stress markers in different studied groups.

3.2. Determination of median survival time.

As presented in Table 3, the mean survival time (MST) was significantly prolonged in both the ZnO NP– and CAO–ZnO NP–treated groups compared with the control group, indicating a positive therapeutic effect. Furthermore, the greater increase in MST observed in

the CAO–ZnO NP–treated group suggests enhanced antitumor efficacy relative to treatment with ZnO NPs alone. Figure 3 shows the median survival time in the different studied groups.

Table 3. Median survival time in the different studied groups.

Parameter	Control	ZnONPs	CAO. ZnONPs	P value	Post hoc
MST	24.6±2.1	42.5±9.5	51±2.3	**P<0.001**	**P1<0.001** **P2<0.001** **P3<0.001**

MST: Median survival time.
ZnONPs: Zinc oxide nanoparticles.
CAO-ZnONPs: Citrus aurantium oil-loaded zinc oxide nanoparticles.
P1: Comparison between the control group and the ZnONPs-treated group.
P2: Comparison between the ZnONPs-treated group and the CAO-ZnONPs-treated group.
P3: Comparison between the CAO-ZnONPs-treated group and the control group.

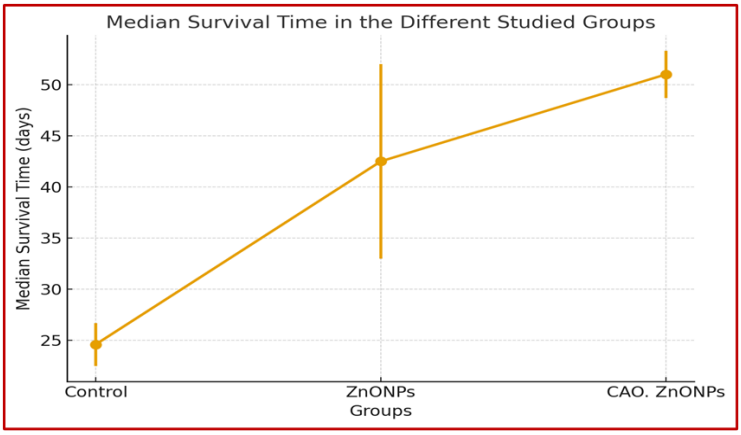

Figure 3. A chart showing median survival time in the different studied groups.

3.3. Determination of apoptotic and inflammatory markers.

As shown in Table 4, the levels of caspase-3, annexin, and tumor necrosis factor-alpha (TNF-α) were significantly reduced in both the ZnO NP– and CAO–ZnO NP–treated groups, indicating a decrease in apoptotic and inflammatory activity.

Table 4. Apoptotic and inflammatory markers in the different studied groups.

Parameter	Control	ZnONPs	CAO. ZnONPs	P value	Post hoc
Caspase-3	2.1±0.2	0.91±0.07	0.55±0.06	**P<0.001**	**P1<0.001** P2=0.001 **P3<0.001**
Annexin	1.9±0.29	0.92±0.16	0.49±0.09	**P<0.001**	**P1<0.001** P2=0.006 **P3<0.001**
TNFα	283.1±21.5	139.2±8.9	70.8±9.1	**P<0.001**	**P1<0.001** **P2<0.001** **P3<0.001**
BCL-2	148.1±16.2	236.3±14.2	272.6±14.2	**P<0.001**	**P1<0.001** P2=0.002 **P3<0.001**

TNF-α: Tumor necrosis factor-alpha;
BCL-2: B-cell lymphoma-2 protein;
ZnONPs: Zinc oxide nanoparticles;
CAO-ZnONPs: Citrus aurantium oil-loaded zinc oxide nanoparticles.
P1: Comparison between the control group and the ZnONPs-treated group.
P2: Comparison between the ZnONPs-treated group and the CAO-ZnONPs-treated group.
P3: Comparison between the CAO-ZnONPs-treated group and the control group.

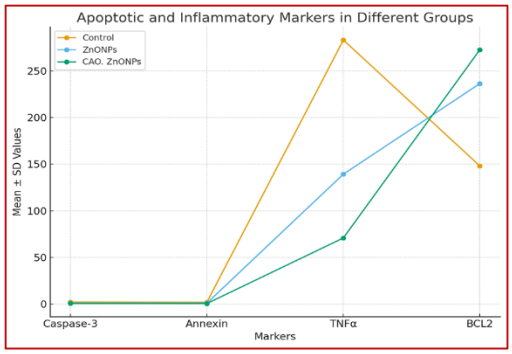

Figure 4. A chart showing apoptotic and inflammatory markers in different groups.

3.4. Determination of kidney and liver function.

As presented in Table 5, blood urea and serum creatinine levels were significantly reduced in both the ZnO NP– and CAO–ZnO NP–treated groups compared with the control group, indicating improved renal function and reduced nephrotoxic stress in the treated animals. These findings suggest a potential protective effect of ZnO NPs, particularly the CAO–ZnO NP formulation, on kidney function. Similarly, serum alanine aminotransferase (ALT) and aspartate aminotransferase (AST) activities were significantly lower in the ZnO NP– and CAO–ZnO NP–treated groups relative to controls, suggesting that both treatments exert a beneficial influence on hepatic function. Figure 5 shows kidney and liver function tests for the different studied groups.

Table 5. Kidney and liver function tests in the different studied groups.

Parameter	Control	ZnONPs	CAO. ZnONPs	P value	Post hoc
Blood Urea (mg/dl)	86.7±4.6	67.9±6.7	45.5±7.9	**P<0.001**	**P1<0.001 P2<0.001 P3<0.001**
Serum Creatinine (mg/dl)	1.3±0.17	1.1±0.16	0.92±0.09	**P<0.001**	**P1=0.018 P2=0.079 P3<0.001**
ALT (U/L)	212.1±49.7	136.3±31.8	80.1±25	**P<0.001**	**P1=0.008 P2=0.047 P3<0.001**
AST (U/L)	494.6±97.4	267.8±54.6	148.1±30.42	**P<0.001**	**P1<0.001 P2=0.019 P3<0.001**

ZnONPs: Zinc oxide nanoparticles;
CAO-ZnONPs: Citrus aurantium oil-loaded zinc oxide nanoparticles;
P1: Comparison between the control group and the ZnONPs-treated group;
P2: Comparison between the ZnONPs-treated group and the CAO-ZnONPs-treated group;
P3: Comparison between the CAO-ZnONPs-treated group and the control group.

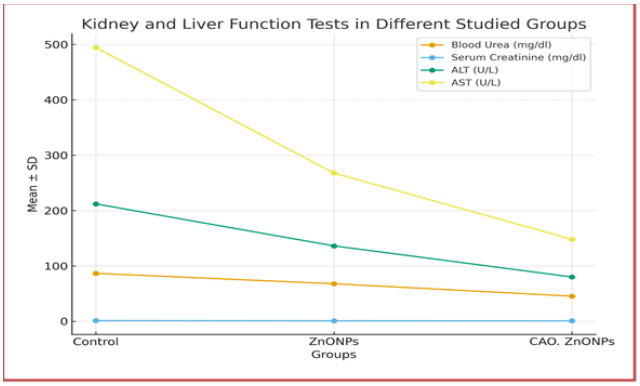

Figure 5. A chart showing kidney and liver function test results across the different study groups.

3.5. Determination of tumor volume.

The data presented in Table 6 demonstrate the superior efficacy of CAO–ZnO NPs in suppressing tumor growth over a 20-day period compared with both the control and ZnO NP–treated groups. At baseline (day 0), all groups exhibited comparable tumor volumes; however, significant differences became evident as the experiment progressed. The control group showed the most rapid increase in tumor volume, whereas the ZnO NP–treated group exhibited a moderate reduction in tumor growth rate. Notably, the CAO–ZnO NP–treated group displayed the smallest increase in tumor volume at all recorded time points, indicating a pronounced inhibitory effect on tumor progression, as illustrated in Figure 6.

Figure 6 further reveals a statistically significant difference between the CAO–ZnO NP and ZnO NP groups, suggesting that functionalization with *Citrus aurantium* oil enhances the antitumor efficacy of ZnO NPs. By day 20, the tumor volume in the control group (1063.2 ± 135.7 mm^3) was markedly higher than that in the CAO–ZnO NP–treated group (297.7 ± 13.5 mm^3), underscoring the strong therapeutic potential of CAO–ZnO NPs as an effective antineoplastic agent. Figure 7 illustrates tumor volume progression over 20 days post-treatment with ZnONPs and CAO-ZnONPs in EAC-bearing mice. Data points represent mean ± SD (n=10 per group). CAO-ZnONPs demonstrated significantly reduced tumor volume compared to both the control and ZnONPs groups at all time points after day 5 ($p < 0.05$).

Table 6. Tumor volume at different intervals in the different studied groups.

		Control	ZnONPs	CAO. ZnONPs	P value	Post hoc
Tumor volume (mm^3)	**0 day**	73.2±9.7	82.8±18	84.4±10.7	**P=0.316**	**P1=0.444** P2=0.976 **P3=0.337**
	5 days	269.9±11.2	243.1±27.8	197.9±17.4	**P<0.001**	**P1=0.084** P2=0.004 **P3<0.001**
	10 days	459.9±17.4	290.5±29.9	231.6±16.7	**P<0.001**	**P1<0.001** P2=0.001 **P3<0.001**
	15 days	708.7±32.7	348.4±30.8	273.6±22.5	**P<0.001**	**P1<0.001** P2=0.001 **P3<0.001**
	20 days	1063.2±135.7	474.7±91.3	297.7±13.5	**P<0.001**	**P1<0.001** P2=0.015 **P3<0.001**

ZnONPs: Zinc oxide nanoparticles;
P1: Comparison between the control group and the ZnONPs group;
P2: Comparison between the ZnONPs group and the CAO-ZnONPs group;
P3: Comparison between the CAO-ZnONPs group and the control group.

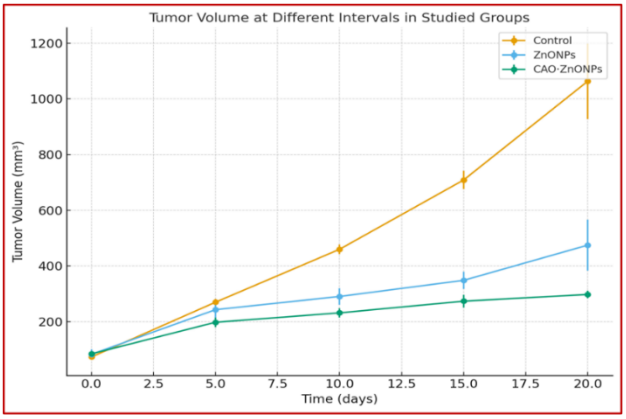

Figure 6. A chart showing tumor volume at different intervals in studied groups.

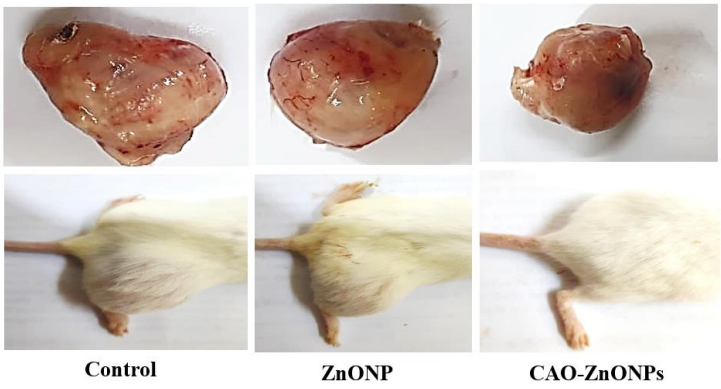

Figure 7. Tumor volume progression over 20 days post-treatment with ZnONPs and CAO-ZnONPs in EAC-bearing mice. Data points represent mean ± SD (n=10 per group). CAO-ZnONPs demonstrated significantly reduced tumor volume compared to both the control and ZnONPs groups at all time points after day 5 ($p < 0.05$).

3.6. Determination of tumor weight.

As shown in Table 7, treatment with both ZnO NPs and CAO–ZnO NPs resulted in a significant reduction in tumor weight compared with the control group. The mean tumor weights were 4.3 g in the control group, 2.9 g in the ZnO NP–treated group, and 2.11 g in the CAO–ZnO NP–treated group, with highly significant differences observed between the control and treatment groups. Among the treated animals, the CAO–ZnO NP group exhibited the greatest reduction in tumor weight, indicating superior antitumor efficacy (Figure 8).

Table 7. Tumor weight in the different studied groups.

	Control	ZnONPs	CAO. ZnONPs	P value	Post hoc
Tumor weight (gm)	4.3±.43	2.9±.51	2.11±.47	**P<0.001**	**P1<0.001** P2=0.024 **P3<0.001**

ZnONPs: Zinc oxide nanoparticles;
P1: Comparison between the control group and the ZnONPs group;
P2: Comparison between the ZnONPs group and the CAO-ZnONPs group;
P3: Comparison between the CAO-ZnONPs group and the control group.

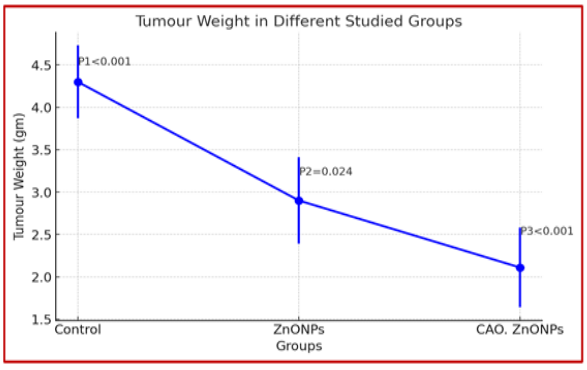

Figure 8. A chart showing tumor weight in the different studied groups.

3.7. Effect of CAO-ZnONPs on the histological structures.

Histopathological examination of the control EAC tumor group revealed extensive areas of necrosis interspersed with viable tumor regions containing numerous mitotic figures, indicating active tumor proliferation. In contrast, the ZnO NP–treated group exhibited smaller viable areas composed of fewer, shrunken neoplastic cells separated by regions of necrosis,

along with occasional multinucleated giant cells and focal calcifications. The CAO–ZnO NP–treated group demonstrated even more pronounced histopathological alterations, characterized by minimal viable tumor regions, a reduced number of shrunken neoplastic cells, broader necrotic zones, and multiple foci of calcification, as illustrated in Figure 9.

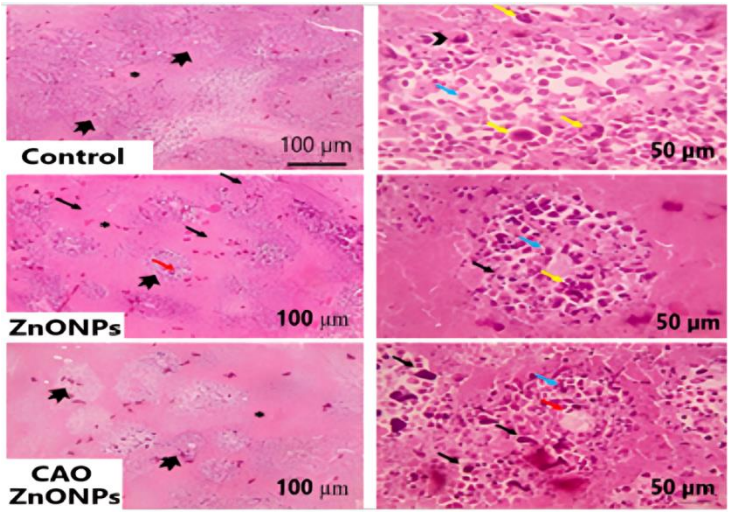

Figure 9. Histopathological analysis of tumor sections stained with H&E. **(A)** Control group: large viable tumor areas, mitotic figures, and pleomorphic nuclei; **(B)** ZnONPs group: moderate necrosis and reduced viable cell population; **(**C) CAO-ZnONPs group: extensive necrosis, minimal viable tumor cells, and evidence of calcification. Magnification: 100x (left), 400x (right). Scale bars: 100 µm and 50 µm, respectively.

3.8. Discussion.

The findings of the present study demonstrate that both zinc oxide nanoparticles (ZnONPs) and *Citrus aurantium* oil-functionalized ZnONPs (CAO-ZnONPs) exhibit pronounced antitumor activity in a murine model of Ehrlich ascites carcinoma (EAC). Notably, treatment with CAO-ZnONPs markedly inhibited tumor progression, enhanced antioxidant capacity, and mitigated inflammatory responses. These therapeutic outcomes may be attributed to the synergistic effects of ZnO-induced oxidative modulation and the inherent bioactive properties of *C. aurantium* oil. Collectively, these results provide a promising foundation for the future development of plant-functionalized nanotherapeutics with improved efficacy and reduced systemic toxicity [6].

Under pathological conditions such as cancer, mitochondrial dysfunction leads to impaired ATP synthesis, resulting in metabolic stress. This dysfunction disrupts the redox equilibrium between reactive oxygen species (ROS) generation and antioxidant defense mechanisms. Consequently, excessive lipid peroxidation produces elevated malondialdehyde (MDA) levels, a well-established marker of oxidative stress [13–15]. Catalase (CAT), an essential antioxidant enzyme, decomposes hydrogen peroxide (H_2O_2) into water and oxygen, thereby alleviating oxidative burden [16].

The therapeutic potential of ZnONPs and CAO-ZnONPs appears to involve multifaceted mechanisms encompassing antioxidative, anti-inflammatory, and pro-apoptotic pathways. At the molecular level, ZnONPs exhibit antioxidant properties by significantly reducing MDA levels, a hallmark indicator of lipid peroxidation [17,18]. This reduction underscores the nanoparticles' capacity to neutralize ROS, which are key mediators of DNA damage, mutagenesis, and oncogenic transformation [17–19]. In parallel, the observed elevations in intracellular antioxidants, such as glutathione (GSH) and superoxide dismutase

(SOD), confirm the reinforcement of endogenous antioxidant defenses. The higher antioxidant levels in the CAO-ZnONPs-treated group further suggest that *C. aurantium* oil enhances the antioxidative potency of ZnONPs.

In line with our results, Raajshree and Brindha [20] reported that ZnO-NP treatment reduced tumor volume and prolonged the survival of tumor-bearing mice, while restoring hematological and hepatic biochemical profiles. Furthermore, the concurrent elevation of nitric oxide (NO) and catalase (CAT) activities in treated groups indicates a broader antioxidative influence that integrates ROS buffering with NO-mediated cellular signaling. These pathways play essential roles in modulating apoptosis, angiogenesis, and vascular homeostasis, thereby influencing the tumor microenvironment and metastatic potential.

Consistent with previous studies, ZnO nanoparticles have been shown to induce tumor cell death primarily through ROS generation and suppression of the cellular antioxidant system [21]. Excessive ROS formation leads to depletion of antioxidative enzymes, DNA damage, and apoptotic activation *via* downregulation of Bcl-2 expression [22]. These molecular events culminate in oxidative injury, tumor regression, and cancer cell death.

Inflammation is a critical driver of cancer progression through the promotion of cellular proliferation, angiogenesis, and metastasis. The significant reduction in tumor necrosis factor-alpha (TNF-α) observed following ZnONP treatment suggests attenuation of inflammatory signaling within the tumor microenvironment. These immunomodulatory effects suggest that ZnONPs may reprogram immune activity, thereby depriving tumor cells of pro-survival cues [23]. Ghanem *et al*. [21] similarly reported that ZnONP administration significantly decreased inflammatory responses in EAC-bearing mice.

Interestingly, the current study also revealed reductions in caspase-3 and annexin V levels, accompanied by elevated B-cell lymphoma 2 (BCL-2) expression, suggesting a complex modulation of apoptotic pathways. These observations may indicate selective apoptosis in malignant cells, while normal cells are protected through upregulation of anti-apoptotic mechanisms. Supporting this notion, Ghanem *et al*. [21] demonstrated that ZnONPs downregulate Bcl-2 expression in EAC cells, while El-Shorbagy *et al*. [22] confirmed the central role of Bcl-2 in apoptosis regulation and tumor suppression.

Additional studies by Ghaznavi *et al*. [24] and Shishesaz *et al*. [25] further corroborate the cytotoxicity of ZnONPs against cancer cells, reporting concentration-dependent reductions in tumor cell viability with minimal effects on normal tissues.

Histopathological examination in the present study aligns with these biochemical findings. The EAC control group exhibited extensive viable tumor regions with numerous mitotic figures and necrotic areas. In contrast, ZnONP-treated tumors displayed smaller viable regions, with fewer shrunken neoplastic cells interspersed among necrosis and calcification. The CAO-ZnONPs group showed even greater necrotic expansion and cellular degeneration, indicating an enhanced cytotoxic effect.

Taken together, these findings underscore the multi-targeted therapeutic potential of CAO-ZnONPs, which act through a combination of oxidative stress modulation, apoptosis induction, and immune regulation. This integrated mode of action not only inhibits tumor growth but also appears to preserve the integrity of adjacent healthy tissues, highlighting CAO-ZnONPs as a promising platform for the design of safe and effective nanotherapeutic agents.

Oxidative stress is closely linked to programmed cell death (apoptosis). Excessive oxidative stress is a key trigger of apoptosis, as reactive oxygen species (ROS) accumulate and

damage cellular components. While a balanced ROS level helps maintain cell health, an imbalance can initiate apoptosis, contributing to the development of various diseases.

3.9. Mechanisms by which oxidative stress induces apoptosis.

An imbalance between the generation of reactive oxygen species (ROS) and the antioxidant defense system is known as oxidative stress, and it is a key factor in determining the fate of cancer cells. Due to increased metabolic activity and genetic changes, elevated ROS levels are often observed during carcinogenesis and can cause cellular damage and dysfunction. Oxidative stress is a powerful inducer of apoptosis, a strictly controlled process of planned cell death, even though it may also trigger biological reactions, including DNA damage. Key apoptotic signaling pathways, such as mitochondrial dysfunction, caspase activation, and regulation of Bcl-2 family proteins, are triggered by the accumulation of ROS. Furthermore, oxidative stress can activate the tumor suppressor protein p53, which further induces apoptosis via both transcription-dependent and independent pathways. In cancer cells, dysregulation of these apoptotic pathways can promote tumor growth and treatment resistance. Potential therapeutic insights for addressing oxidative damage in cancer treatment can be gained by comprehending the relationship between oxidative stress and apoptosis [26].

4. Conclusions

The present study demonstrates that *Citrus aurantium* oil–functionalized zinc oxide nanoparticles (CAO–ZnONPs) represent a promising nanotherapeutic approach for cancer management. In addition to effectively reducing tumor burden, these nanoparticles enhance hepatic and renal function and favorably modulate oxidative stress and inflammatory pathways. These findings underscore the potential of plant-based nanoparticle formulations as safer and more targeted alternatives to conventional chemotherapy. Future investigations should focus on long-term safety, biodistribution, and the translational potential of CAO–ZnONPs for clinical applications.

Author Contributions

Conceptualization, L.A.A.B. and N.M.H.; methodology, L.A.A.B.; software, N.M.H. and A.S.E.; validation, A.S.E. and L.A.A.B.; formal analysis, A.S.E. and L.A.A.B.; investigation, L.A.A.B. and N.M.H.; resources, L.A.A.B., N.M.H., and A.A.A.; data curation, A.S.E.; writing—original draft preparation, A.S.E. and A.A.A.; writing—review and editing, A.S.E. and L.A.A.B.; visualization, A.S.E.; supervision, L.A.A.B. and N.M.H.; project administration, L.A.A.B. and N.M.H.; funding acquisition, A.S.E. All authors have read and agreed to the published version of the manuscript.

Institutional Review Board Statement

All care and procedures used in the present study were in accordance with the NIH Guide, and animals were used with the approval of the Ethics Committee at the Faculty of Science, Port Said University, which approved this research on 13/08/2023.

Informed Consent Statement

Not applicable, as this study did not involve human subjects.

Data Availability Statement

All data generated or analyzed during this study are included in this published article.

Funding

This research received no specific grant from funding agencies in the public, commercial, or not-for-profit sectors.

Acknowledgment

Nil.

Conflicts of Interest

The authors declare that they have no conflict of interest..

Abbreviations

The following abbreviations are used in this manuscript:

Abbreviation	Definition
CAO	*Citrus aurantium* oil
ZnONPs	Zinc oxide Nanoparticles
FT-IR	Fourier Transform Infrared Spectroscopy
UV-vis	Ultraviolet and Visible Spectra
XRD	X-ray Powder Diffraction
TEM	Transmission Electron Microscope
HRTEM	High-Resolution Transmittance Electron Microscope
SAED	Selected Area Electron Diffraction
ROS	Reactive Oxygen Species
EAC	Ehrlich Ascites Carcinoma
PBS	Phosphate-Buffered Saline
ELISA	Enzyme-Linked Immunosorbent Assay
ALT	Alanine Transaminase
AST	Aspartate Aminotransferase

References

1. Obafemi, F.A.; Umahi-Ottah, G. A review of global Cancer prevalence and therapy. *J. Cancer Res. Treat. Prev* **2023**, *1*, 128-147, https://doi.org/10.37191/Mapsci-JCRTP-1(3)-011.
2. Sung, H.; Ferlay, J.; Siegel, R.L.; Laversanne, M.; Soerjomataram, I.; Jemal, A.; Bray, F. Global Cancer Statistics 2020: GLOBOCAN Estimates of Incidence and Mortality Worldwide for 36 Cancers in 185 Countries. *CA Cancer J. Clin.* **2021**, *71*, 209-249, https://doi.org/10.3322/caac.21660.
3. Wang, M.D.; Simons, J.W.; Nie, S. Cancer Nanotechnology for Molecular Profiling and Individualized Therapy. In Pharmacogenetics of Breast Cancer, 1st Edition; Leyland-Jones, B., Ed.; CRC Press: Boca Raton, **2020**; p. 309-322, https://doi.org/10.1201/9780429137723-20.
4. Vaghari-Tabari, M.; Jafari-Gharabaghlou, D.; Mohammadi, M.; Hashemzadeh, M.S. Zinc Oxide Nanoparticles and Cancer Chemotherapy: Helpful Tools for Enhancing Chemo-sensitivity and Reducing Side Effects?. *Biol. Trace Elem. Res.* **2024**, *202*, 1878-1900, https://doi.org/10.1007/s12011-023-03803-z.
5. Anjum, S.; Hashim, M.; Malik, S.A.; Khan, M.; Lorenzo, J.M.; Abbasi, B.H.; Hano, C. Recent Advances in Zinc Oxide Nanoparticles (ZnO NPs) for Cancer Diagnosis, Target Drug Delivery, and Treatment. *Cancers* **2021**, *13*, 4570, https://doi.org/10.3390/cancers13184570.
6. Donmez, S.; Keyvan, E. Green synthesis of zinc oxide nanoparticles using grape seed extract and evaluation of their antibacterial and antioxidant activities. *Inorg. Nano-Metal Chem.* **2024**, *54*, 1137–1144, https://doi.org/10.1080/24701556.2023.2165687.

7. Erdoğan, Ö.; Paşa, S.; Demirbolat, G.M.; Birtekocak, F.; Abbak, M.; Çevik, Ö. Synthesis, characterization, and anticarcinogenic potent of green-synthesized zinc oxide nanoparticles via Citrus aurantium aqueous peel extract. *Inorg. Nano-Metal Chem.* **2025**, *55*, 67-75, https://doi.org/10.1080/24701556.2023.2240768.
8. Hosny, N.M.; Eissa, A.S.; Awadalla, A.A.; Barakat, L.A.A. Synthesis, Anti-oxidant and Cytotoxicity Activity of ZnO Nanoparticles Wrapped with *Citrus aurantium*. *Lett. Appl. NanoBioSci.* **2024**, *13*, 177, https://doi.org/10.33263/LIANBS134.177.
9. Nguyen, P.A.H.; Clark, E.R.; Ananthakrishnan, S.; Lenz, K.; Canavan, H.E. How to select the appropriate method(s) of cytotoxicity analysis of mammalian cells at biointerfaces: A tutorial. *Biointerphases* **2020**, *15*, 031201, https://doi.org/10.1116/6.0000136.
10. Goleij, P.; Rezaee, A.; Lam, H.Y.; Tabari, M.A.K.; Ouf, N.; Alijanzadeh, D.; Sanaye, P.M.; Larsen, D.S.; Daglia, M.; Khan, H.; Sethi, G.; Kumar, A.P. From bench to bedside: exploring curcumin-driven signaling pathways in immune cells for cancer management. *Inflammopharmacology* **2025**, *33*, 2293-2306, https://doi.org/10.1007/s10787-025-01739-5.
11. Hao, Y.; Wang, Y.; Zhang, L.; Liu, F.; Jin, Y.; Long, J.; Chen, S.; Duan, G.; Yang, H. Advances in antibacterial activity of zinc oxide nanoparticles against Staphylococcus aureus (Review). *Biomed. Rep.* **2024**, *21*, 161, https://doi.org/10.3892/br.2024.1849.
12. Kafali, M.; Finos, M.A.; Tsoupras, A. Vanillin and Its Derivatives: A Critical Review of Their Anti-Inflammatory, Anti-Infective, Wound-Healing, Neuroprotective, and Anti-Cancer Health-Promoting Benefits. *Nutraceuticals* **2024**, *4*, 522-561, https://doi.org/10.3390/nutraceuticals4040030.
13. Manohar, S.; Leung, N. Cisplatin nephrotoxicity: a review of the literature. *J. Nephrol.* **2018**, *31*, 15-25, https://doi.org/10.1007/s40620-017-0392-z.
14. Ling, L.; Feng, X.; Wei, T.; Wang, Y.; Wang, Y.; Zhang, W.; He, L.; Wang, Z.; Zeng, Q.; Xiong, Z. Effects of low-intensity pulsed ultrasound (LIPUS)-pretreated human amnion-derived mesenchymal stem cell (hAD-MSC) transplantation on primary ovarian insufficiency in rats. *Stem Cell Res. Ther.* **2017**, *8*, 283, https://doi.org/10.1186/s13287-017-0739-3.
15. Da-silva, O.F.; Adelowo, A.R.; Babalola, A.A.; Ikeji, C.N.; Owoeye, O.; Rocha, J.B.T.; Adedara, I.A.; Farombi, E.O. Diphenyl Diselenide Through Reduction of Inflammation, Oxidative Injury and Caspase-3 Activation Abates Doxorubicin-Induced Neurotoxicity in Rats. *Neurochem. Res.* **2024**, *49*, 1076-1092, https://doi.org/10.1007/s11064-023-04098-1.
16. Yurttancikmaz, E.T.; Ozcan, P.; Tanoglu, F.B.; Tok, O.E.; Timur, H.T.; Cetin, C. Protective Effect of Glutathione Administration on Ovarian Function in Female Rats with Cyclophosphamide-Induced Ovarian Damage. *Gynecol. Obstet. Invest.* **2024**, *89*, 120-130, https://doi.org/10.1159/000536055.
17. Rehman, H.; Ali, W.; Zaman Khan, N.; Aasim, M.; Khan, T.; Ali Khan, A. *Delphinium uncinatum* mediated biosynthesis of zinc oxide nanoparticles and *in-vitro* evaluation of their antioxidant, cytotoxic, antimicrobial, anti-diabetic, anti-inflammatory, and anti-aging activities. *Saudi J. Biol. Sci.* **2023**, *30*, 103485, https://doi.org/10.1016/j.sjbs.2022.103485.
18. Shah, T.; Surendar, S.; Singh, S. Green Synthesis of Zinc Oxide Nanoparticles Using Ananas comosus Extract: Preparation, Characterization, and Antimicrobial Efficacy. *Cureus* **2023**, *15*, e47535, https://doi.org/10.7759/cureus.47535.
19. Chaudhary, P.; Janmeda, P.; Docea, A.O.; Yeskaliyeva, B.; Abdull Razis, A.F.; Modu, B.; Calina, D.; Sharifi-Rad, J. Oxidative stress, free radicals and antioxidants: potential crosstalk in the pathophysiology of human diseases. *Front. Chem.* **2023**, *11*, 1158198, https://doi.org/10.3389/fchem.2023.1158198.
20. Raajshree, R.K.; Brindha, D. *In Vivo* Anticancer Activity of Biosynthesized Zinc Oxide Nanoparticle using *Turbinaria conoides* on a Dalton's Lymphoma Ascites Mice Model. *J. Environ. Pathol. Toxicol. Oncol.* **2018**, *37*, 103-115, https://doi.org/10.1615/JEnvironPatholToxicolOncol.2018025086.
21. Ghanem, H.B. Impact of zinc oxide nanoparticles and thymoquinone in Ehrlich ascites carcinoma induced in mice. *J. Biochem. Mol. Toxicol.* **2021**, *35*, e22736, https://doi.org/10.1002/jbt.22736.
22. El-Shorbagy, H.M.; Eissa, S.M.; Sabet, S.; El-Ghor, A.A. Apoptosis and oxidative stress as relevant mechanisms of antitumor activity and genotoxicity of ZnO-NPs alone and in combination with N-acetyl cysteine in tumor-bearing mice. *Int. J. Nanomed.* **2019**, *14*, 3911-3928, https://doi.org/10.2147/IJN.S204757.
23. Aboulhoda, B.E.; Abdeltawab, D.A.; Rashed, L.A.; Abd Alla, M.F.; Yassa, H.D. Hepatotoxic Effect of Oral Zinc Oxide Nanoparticles and the Ameliorating Role of Selenium in Rats: A histological, immunohistochemical and molecular study. *Tissue Cell* **2020**, *67*, 101441, https://doi.org/10.1016/j.tice.2020.101441.

24. Ghaznavi, H.; Hajinezhad, M.R.; Hesari, Z.; Shirvaliloo, M.; Sargazi, S.; Shahraki, S.; Saberi, E.A.; Sheervalilou, R.; Jafarinejad, S. Synthesis, characterization, and evaluation of copper-doped zinc oxide nanoparticles anticancer effects: in vitro and in vivo experiments. *BMC Cancer* **2025**, *25*, 37, https://doi.org/10.1186/s12885-024-13398-w.
25. Shishesaz, P.; Mahdavi, M.; Ghodratpour, F.; Baghbani-arani, F. Evaluation of Cytotoxic and Apoptotic Effects of Green Synthesized Zn Oxide Nanoparticles on the MCF-7 breast cancer Cell Line. *Koomesh* **2023**, *25*, 270-278, https://doi.org/10.5555/20230331259.
26. Jomova, K.; Alomar, S.Y.; Valko, R.; Liska, J.; Nepovimova, E.; Kuca, K.; Valko, M. Flavonoids and their role in oxidative stress, inflammation, and human diseases. *Chem. Biol. Interact.* **2025**, *413*, 111489, https://doi.org/10.1016/j.cbi.2025.111489.

Publisher's Note & Disclaimer